White Beam Lasing from a Hybrid Microcavity with Slab-Capillary Mode Coupling

Hai-Lang Dai,[1,2] Cheng Yin,[3] Zhi-yuan Xiao,[1,2] Zhuang-Qi Cao,[1] and Xian-Feng Chen[1,2,*]

[1] *The State Key Laboratory on Fiber Optic Local Area Communication Networks and Advanced Optical Communication Systems, School of Physics and Astronomy, Shanghai Jiao Tong University, Shanghai 200240, China*

[2] *Collaborative Innovation Center of IFSA (CICIFSA), Shanghai Jiao Tong University, Shanghai 200240, China*

[3] *Jiangsu Key Laboratory of Power Transmission and Distribution Equipment Technology, Hohai University, Changzhou 213022, China*

(Received 22 February 2019; revised manuscript received 10 April 2019; published 24 June 2019)

We report a hybrid multichannel metal-cladded slab-capillary microcavity, which supports simultaneous red, green, and blue lasing from an individual microcavity at room temperature. White and tunable lasing over the full range of visible colors is achieved through controlled injection of different dye solutions into the metal-cladded capillaries of the microcavity. The results show that RGB lasing beams with a line width of approximately 1 nm are observed from the metal-cladded slab-capillary microcavity. The experimental observations show the realization of white light and lasing simultaneously in a single hybrid microcavity. Moreover, the improvement in the laser structure enables the elimination of background noise. Our work describes a simplification in fabricating microlasers with dynamically color-controllable emissions and provides an important route toward the potential of realizing a microlaser device generating both white and full color light directly from a single monolithic structure.

DOI: 10.1103/PhysRevApplied.11.064055

I. INTRODUCTION

The generation of multiple wavelength (i.e., multicolor) lasing over a wide wavelength span on a single microchip has attracted great interest in recent years, moving toward a white-light laser. The lasing action spanning the full visible spectrum, in particular, red, green, and blue (RGB), is especially useful for laser lighting, full-color laser imaging and displaying, as well as biological and chemical sensing [1–5]. As the illumination source, lasers offer higher energy conversion efficiencies and potentially higher output powers than white light-emitting diodes (LEDs) and other traditional light sources. Moreover, broadly tunable lasers may be used in many applications such as alternative optical interconnects or multiplexing [1], multiagent chemical [2] and biological detection [3], solid-state lighting [4], solar cells [5], and superbright microdisplays [6].

It has recently been demonstrated [2] that generating wavelength flexible and controllable lasers with large wavelength tunability is fundamentally difficult in a conventional approach based on the planar growth technology due to the lattice mismatching. Emissions at the wavelength covering the entire range of the visible light in a single structure requires the growth of potentially very dissimilar semiconductors into monolithic structures with a high crystal quality. Unfortunately, this method of achieving wavelength variability is strongly limited with current methods of growing planar epitaxial heterostructures of semiconductor thin films on a crystalline substrate. Moreover, the growth of the alloy materials requires strain-free conditions without lattice mismatches, which intrinsically prohibits the generation of the desired lasers [7].

Alternatively, developments in nanotechnology over the past two decades have shown the possibilities of generating emissions over a wide spectral range by using quantum dots and nanowires as means of producing emissions over a wide spectral range. However, quantum dots is made with solution-based techniques, it is still difficult for avoiding the absorption of emissions at the short wavelength by narrow-gap dots by controlling their spatial distribution [8]. Most of the previous approaches use nonsemiconductor materials such as nonlinear crystals [7,9–11], rare-earth-doped materials [8,12,13], dye-doped polymers [14] and liquids [15], and microfibers [16–20]. Furthermore, the bulk setup with quantum dots is incompatible with the electrical injection, which prohibits possible applications in the field of integrated photonics. Therefore, it is of fundamental importance to achieve a compatible multichannel cavity structure with a high quality factor, which generates simultaneous lasing at three primary or multielementary

*xfchen@sjtu.edu.cn

colors. In addition, a metal-cladded slab-capillary mode-cross-coupled microcavity (i.e., a hybrid microcavity) holds promise for strongly enhancing the emission at the ultralow threshold.

It has been shown that one-color lasing as well as narrowband coherent light emission can be demonstrated in a "macroscale" optofluidic waveguide cavity [21]. Nevertheless, compared to the directional output in a conventional laser, a concentric conelike emission in the vertical direction from the surface of the cavity prohibits it being a useful dye-lasing source [22]. We have demonstrated that in the resonance cavity with its dimensionality much larger than the wavelength scale, the pump threshold can be significantly reduced if one introduces an asymmetrical metal-cladded waveguide (SMCW) structure to enhance the excitation of the resonance modes in the gain medium. This waveguide chip includes a millimeter-thick resonance cavity filled with active medium, which supports thousands of guided modes, that is, ultrahigh-order modes (UOMs) [23]. At small incident angles, the standing optical field oscillates rapidly across the linear cavity between the metallic coupling layer and substrate, resulting in various interesting properties, such as strong field enhancement, high sensitivity, and polarization independence [24]. However, since there is only one single channel on the chip and a strong background fluorescence, monochromatic lasing is obtained due to difficult direct detection in incident space. Furthermore, the emission of monochromatic lasing has been scattered to produce a series of concentric light rings [25]. Therefore, here, we improve the structure to eliminate background noise and integrated multiple capillaries on the slab, which forms a multichannel hybrid microcavity with low background noise to achieve multiple-wavelength lasing.

In this article, we show a hybrid microcavity composed of a submillimeter symmetrical metal-cladded slab waveguide (SMSW) and a hollow-core capillary. Capillary oscillations are governed by surface tension and are, therefore, distinguished from acoustic oscillations. These oscillations play a major role in microstructure coalescence and are also important phenomena in interface theories. Moreover, the metal-cladding structure outside of the capillary couples the intrinsic modes with the SMSW transmission modes, and hence traps these modes inside the hollow core of the capillary. Therefore, a resonant electric field with a high density is formed in the hollow core. Such a design is capable of excitation of the capillary eigenmodes by the UOMs of the SMSW. In our numerical simulations, the incident light is coupled into the waveguide layer with a specific coupling angle obtained by solving the mode eigenvalue equation of the SMSW [26]. With a small incident angle, which gives a minimum effective index difference between the adjacent modes over the whole waveband, the final SMSW design supports more than 1000 modes, indicating fully lifted eigenmode channels for the SMSW transmission. Feedback provided by the total internal reflection on the structure surface leads to a laser emission at discrete wavelengths with high Q resonances inside the gain medium profile of the dye solutions.

II. STRUCTURAL CHARACTERIZATION

The waveguide structure of the microcavity chip [Fig. 1(a)] is 10-mm long and 7-mm wide, including a 0.1-mm-thick glass slab as the base of the chip. The upper and lower surfaces of the glass slab are parallel (less than 4″). The glass slab and a capillary with an outside radius of 0.1 mm are used as guiding layers. A thin silver film (about 40-nm thick) on the upper layer is used to couple the pump light into the waveguide. Another 300-nm-thick silver film serves as a substrate layer. We excite the UOMs in the chips with and without the capillary, and for the chip with the capillary, the UOMs are coupled inside the capillary. The spectral reflectance in the slab (slab-capillary) waveguide, R_1 (R_2), is experimentally measured as a function of the incident angle in the range of 0°–5° [Figs. 1(c)–1(f)].

We compare the spectral reflectances R_1 and R_2. Over the same range of the incident angle, the numbers of modes indicated by the dips in the spectral reflectances (R_1 and R_2) are different for two kinds of waveguides. Note that coupling angles, (defined by the incident angle at the resonant dips in the spectral reflectance), as well as the FWHMs of the modes are also different for two spectra, R_1 and R_2. Clearly, the FWHM in spectrum R_2 is less than that in spectrum R_1 [Figs. 1(d) and 1(f)]. To understand the experimental phenomena shown above, we use the standard optical waveguide theory to explain and analyze the results. For an optical waveguide consisting of a thick guiding layer and two metal-cladding layers, the reduced dispersion equation for UOMs is $k_0 h\sqrt{n^2 - N^2} = m\pi$, where $k_0 = 2\pi/\lambda$ is the propagation constant in vacuum; h and n are the thickness and refractive index of the waveguide layer, respectively; $N = \beta/k_0$ is the effective refractive index, $\beta = k_0 n \sin\theta$ is the propagation constant of the guiding modes; m is an integer giving the chosen mode [27].

Except for high-order modes, the effective refractive index of the UOMs N in SMCW is extremely small and is usually less than the refractive index of air. Hence, the number of modes is controlled by the thickness h and the refractive index of the guide layer n, $m \propto h$, n. Therefore, the slab and slab-capillary structures have different thicknesses, h_1 and h_2 ($h_1 < h_2$), resulting in m_1 for the slab waveguide being less than m_2 for the slab-capillary waveguide, which is consistent with the experiments. To excite the cavity mode for lasing, as well as to characterize the optical and cavity modes, light from a tunable laser is coupled into the hybrid microcavity using the slab layer, which is also used to guide the light out from the hybrid

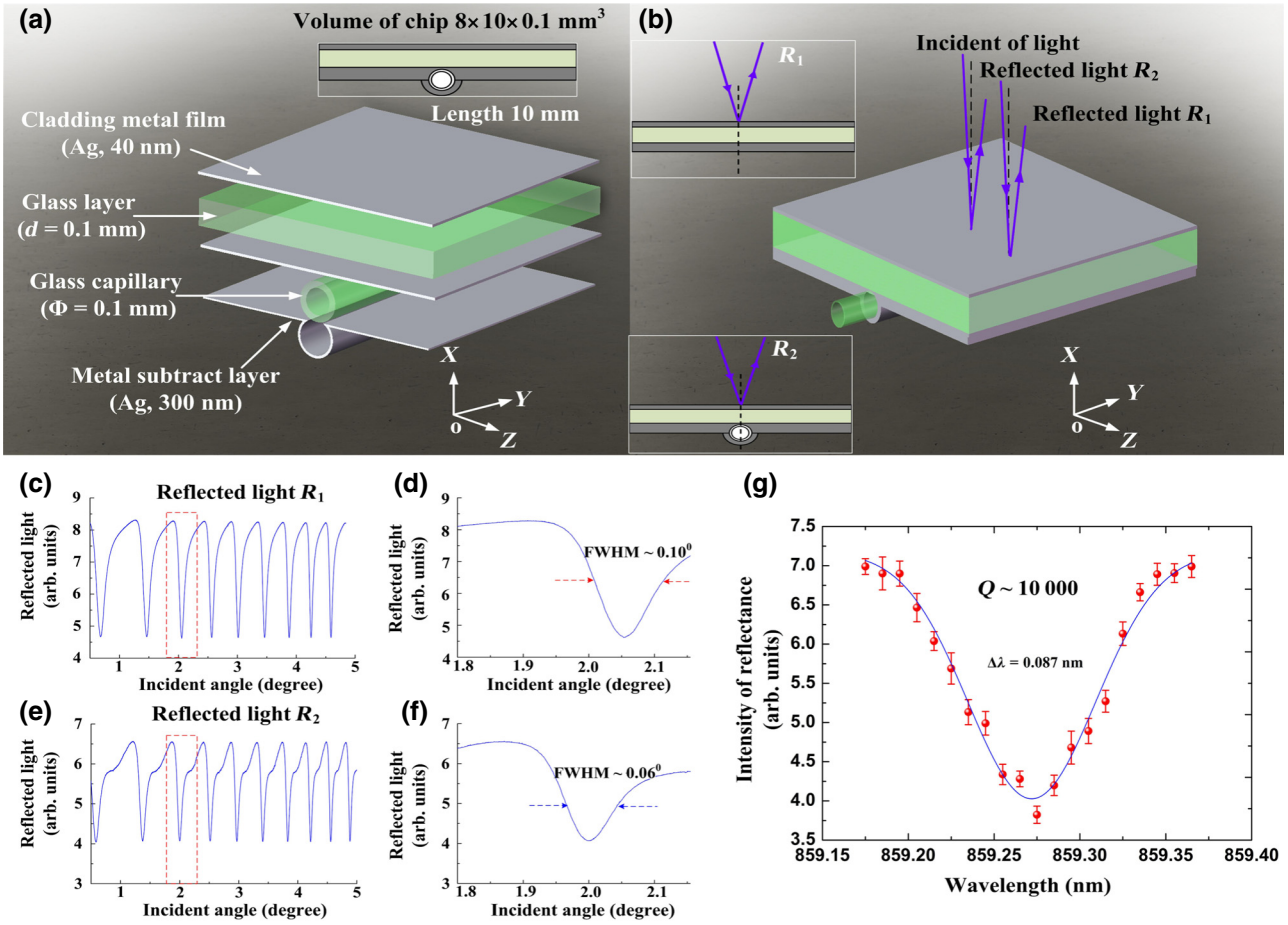

FIG. 1. Structure of the slab-capillary mode-cross-coupled microcavity. (a) Schematic diagram of the hybrid microcavity. The thickness of the coupling layer ranges from 30 to 50 nm, and the metal substrate is about 300 nm. The guiding layer includes a capillary with a radius of 0.1 mm and glass slab with a thickness of 0.1 mm. (b) Excitation of the UOMs via free space coupling technique in slab waveguide (reflectance R_1) and slab-capillary waveguide (reflectance R_2). (c),(e) Reflectance spectra of the modes for the slab waveguide and the slab-capillary waveguide, respectively, versus the incident angle. (d),(f) are the corresponding enlarged plots. (g) The measurement of the resonance reflectance, indicating the optical quality factor.

microcavity and into the detector. The quality factor Q of the cavity mode for this microcavity is 10^4 [see Fig. 1(g)].

III. THEORY AND SIMULATION OF STRUCTURE

Our waveguide chip is different from the conventional Fabry–Perot resonator in many aspects. First of all, the effective refractive index of the guiding modes in our structure approaches zero, which is independent of the specific design of the guiding layer. Moreover, different from the result in Ref. [27], there is no propagating plasmon wave existing in our devices because we directly couple the light into the chip from the free space without a high-index prism [Fig. 1(b)]. In the guiding layer, the resonance modes oscillate at the high intensity. Numerical simulations indicate that the Poynting vector of the mode is enhanced by sixty times of the incident light [28]. Therefore, the mode density for photons in the resonance UOMs is high. Because the thickness of the guiding layer is three orders of magnitude larger than the wavelength, the difference in transversal wave vectors between two adjacent modes is small, and hence leads to the high-mode density in our structure, which reveals the physics behind the intermode coupling. To calculate the mode orders m, we take a three-layered model and perform the numerical simulations. The parameters are set as wavelength 473 nm, dielectric constant for silver $\varepsilon_{Ag} = -8.4 + 0.23i$, thickness of the coupling layer 40 nm, guiding layer thickness $d = 1$ mm, and dielectric constant for the guiding layer $\varepsilon_1 = 1.33^2$. The result gives $m = 3373$, and the calculated effective refractive index of the mode is $N \approx 1.064 + 2.492 * 10^{-7}i$. With this piece of information, we further use COMSOL software to simulate the distribution of the field in the guiding layer and the capillary (Fig. 2). When the incident laser beam illuminates the top of the chip surface, its energy is transferred and stored as modes in the guiding layer when

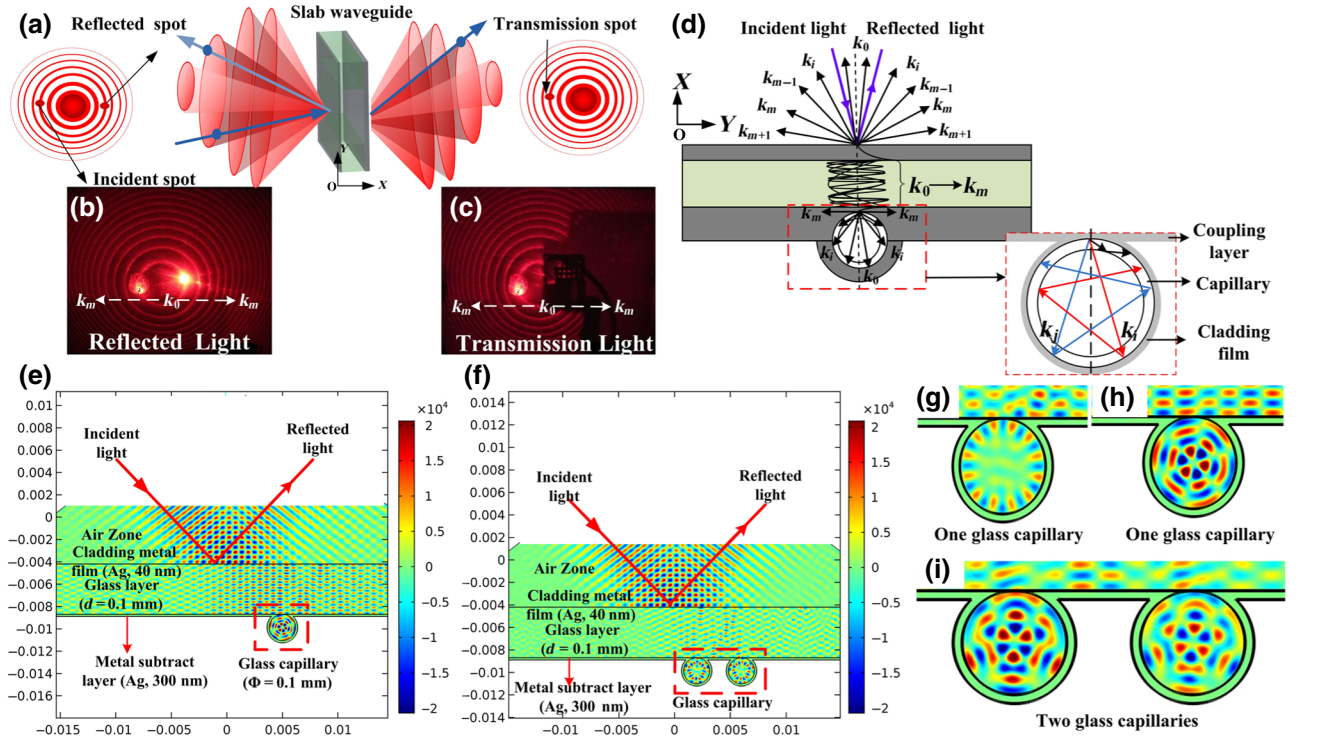

FIG. 2. Theory and simulation of structural modes: (a) A series of reflection and transmission cones in which each cone corresponds to a specific UOM projection from the front and back surfaces of the metal-cladded slab waveguide; (b),(c) Experimental images revealing a series of reflection and transmission cones; (d) Specific UOMs with a fixed wavevector k_m $(m = 0, 1, 2, \ldots)$ from the slab waveguide; (e),(f) COMSOL simulations results in a single slab-capillary microcavity and a double slab-capillary microcavity; (g),(h) Electromagnetic field distributions for the single slab-capillary microcavity and double slab-capillary microcavities, respectively.

the incident angle reaches the coupling angle. Because the upper metallic layer is thin, the energy of all of the UOMs leak out. For each specific UOM with a fixed transverse wavevector k_m $(m = 0, 1, 2, \ldots)$, a concentric light cone is observed since the mode is converted back into a freely propagating light beam, which serves as a leakage radiation source from the coupling layer. This is different from specular reflection, which produces only a bright spot on the screen [29]. Intuitively, a collimated laser beam can only excite one UOM at a certain k_m. Nevertheless, our experimental results reveal a series of reflection and transmission cones, with each cone corresponding to a specific UOM [Figs. 2(a)–2(c)]. As a physical explanation, once the energy of the incident light is coupled and stored in the guiding layer, the leakage radiation takes place throughout all UOM channels and then produces a unique reflection cone. The transmission process inside the resonance cavity is similar and generates the coherent emission with a series of concentric cones at different wavelengths in the experiment.

Thousands of modes are excited at and transmitted through the SMSW, where there is a weak, thin silver film on its back surface. This film plays two crucial roles in the hybrid microcavity, that is, it enables all of the modes transmitted through the film [see Fig. 2(d)] and it acts as a coupling layer of the capillary enabling the majority of these modes to be coupled into the capillary via the bonding area.

To demonstrate that the modes couple into the capillary and induce a standing wave field in the interior of the capillary, we use the COMSOL software, we use simulations done in two different types of structures as shown in Figs. 2(e) and 2(f), where one has a single capillary and the other has two capillaries bonded to the slab. The incident light has a Gaussian profile at a wavelength of 632.8 nm. The incident angle is chosen as the coupling angle and is calculated by using the attenuated total-reflectance software. The simulation results show that our structure supports the strong density in the slab waveguide and capillary indicating the possibility of achieving lasing emission when the cavity is filled with gain medium.

Furthermore, to show the potential of generating multicolor lasing emissions in a single chip, we design a slab-capillary microcavity with different channel configurations by changing the number of capillaries. We perform COMSOL simulations to analyze the cavity modes in our structure and the parameters of the structure are set to be the same as the actual values. The distribution of an

electromagnetic field in the interior of the slab waveguide layer and cavity modes of the capillary are described in Figs. 2(g)–2(i). The electromagnetic field is an oscillating wave inside the structure including the slab waveguide layer and the cavity of the capillary. In the boundaries between the metal and the glass, as well as between the metal and the air, fields are an evanescent wave, which acts as the energy transmission bridge between the metal dielectric layer and the nonmetal dielectric layer.

IV. RESULTS

In this study, we conduct experiments with two different waveguide chip structures, where one involves a single capillary and the other involves a triple capillary waveguide chip with simultaneous RGB lasing. The organic dyes are selected such that each supports the emission at the wavelength corresponding to one of the three primary colors [30], that is, stilbene 420 (S-420), coumarin 540 (C-540), and rhodamine 610 (R-610). The three dyes S-420, C-540, and R-610, are ethanol solutions. B simultaneously y pumping the waveguide chip and operating, a white light emission is obtained from the waveguide chip. To avoid bleaching, the dye solution is continuously injected into the channel through the inlet using a syringe pump (PHD 2000, Harvard Apparatus). In our experiment, we find that the balance among the three dye solutions gives the condition of S-420 0.75, C-540 0.51, and R-610 1.5 mmol/L.

To obtain single wavelength lasing, we inject a dye solution into the cavity of the single capillary waveguide chip with a syringe pump. Lasing beams are emitted at the ends of the capillary when each dye solution is injected into the capillary of the waveguide chip [Figs. 3(c)–3(e)]. When the pumping light ($\lambda = 405$ nm, continuous wave diode pumped solid state laser, maximum power 30 mW, spot diameter 1 mm) illuminates the upper surface and we detect a lasing spectrum obtained by using a spectrograph and imaged by a CCD. In addition, along the z direction, the fluorescence intensity nearly fades away at the ends of the capillary. We observe a bright beam of light emitted from the end face, while the broad-band fluorescence is absorbed and leaked into the metal-cladded layer of the capillary. A resonance mode is formed only when cavity modes and transition modes of the fluorescence molecule are the same. Consistent with the laser principle, the mode is confined in the capillary along the z direction of oscillation up to the output end of the capillary. When the pumping power is changed, we observe that the blue, green, and red lasing spectra remain unchanged, and the peak of the lasing intensity decreases as the pump intensity diminishes.

Three capillaries are bonded side by side on the slab waveguide [Fig. 4(b)] with a 300-nm layer of metal cladding. In the interior of these capillaries, we achieve a high power density in the three microcavities. The outside diameter of each capillary is 0.1 mm, and the total width of the three capillaries side by side is 0.3 mm. The pumping

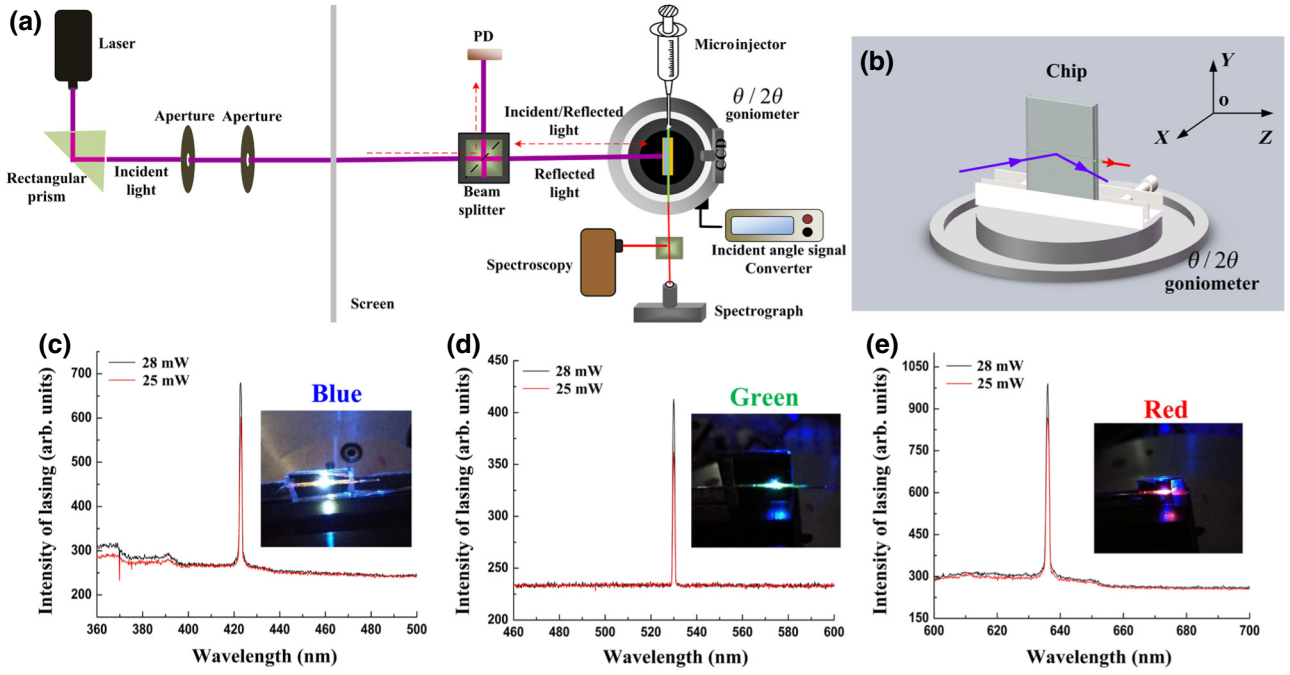

FIG. 3. Experimental system and RGB lasing in a single metal-cladded slab-capillary microcavity: (a) Experimental system and setup. (b) The chip is fixed on the $\theta/2\theta$ goniometer, the rotation of which is controlled by a PC. (c)–(e) Blue, green, and red lasing occurs when pumping lights of 25 and 28 mW power illuminate the silver film on the chip. Inset: images of RGB color lasing.

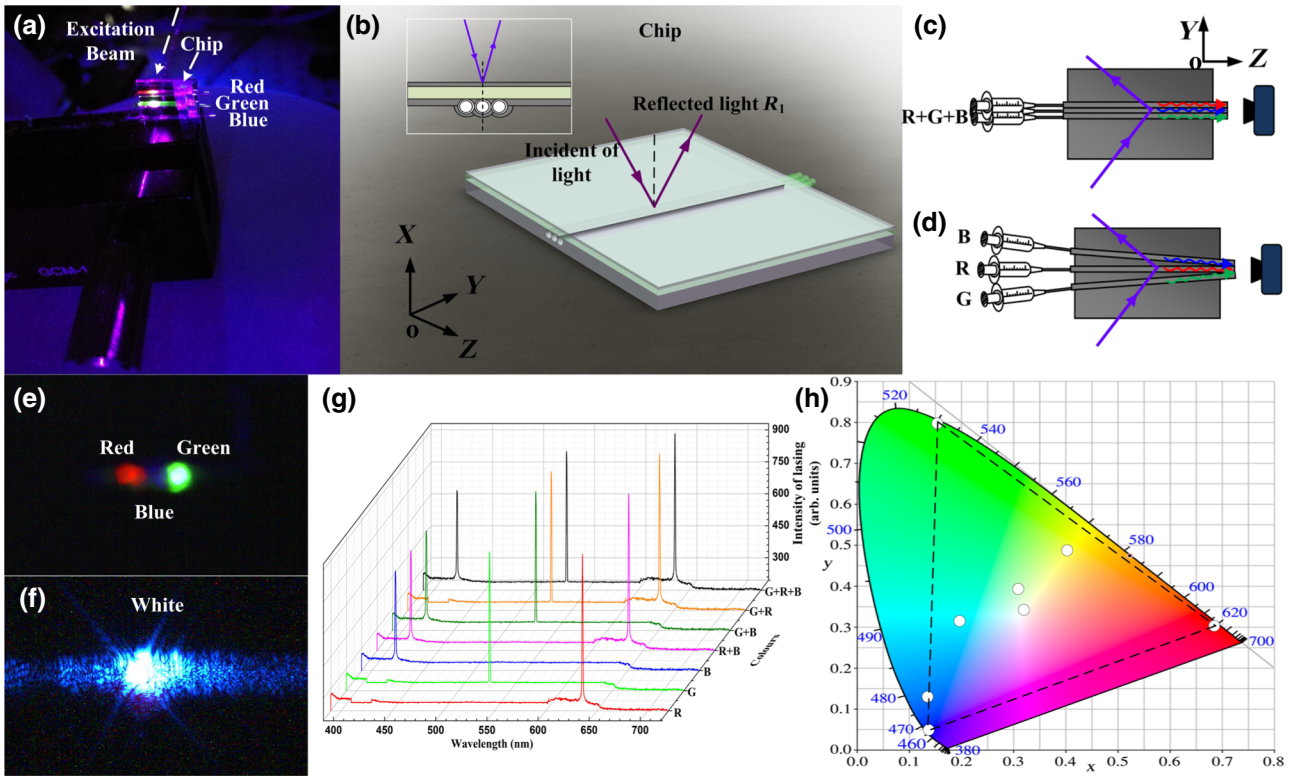

FIG. 4. RGB and white lasing: (a)–(c) The pump beam illuminates the upper surface of the triple hybrid microcavity chip. The three capillaries are placed side by side. S-420, C-540, and R-610 dye solutions are injected into the capillaries. (d) Adjusting the inclination of the capillaries, the RGB lasing beam converges to a point to form a white lasing point. (e) Image shows the RGB lasing points excited side by side in the chip structure. (f) White lasing point. (g) Lasing spectra when the blue (B), green (G), red (R), red and green (R + G), green and blue (G + B), red and blue (R + B) and red, green and blue (R + G + B) segments are pumped above their respective thresholds. (h) Chromaticity of the lasing peaks shown as seven white circles extracted from the spectra in (g). Chromaticity of the R + G + B lasing is close to the CIE standard white illuminant D65. Dashed lines indicate the range of the achievable color palate for this particular chip.

spot with a 1-mm diameter illuminates all three capillaries simultaneously. The energy of the pump field is averaged to each cavity when the three capillaries are fabricated in the metal-cladded slab waveguide. The S-420, C-540, and R-610 dye solutions are injected into their respective capillaries. By pumping above the lasing threshold, we demonstrate one-color lasing of each RGB color, simultaneous two-color lasing of any two of the three primary colors, and finally simultaneous RGB lasing of all three [Figs. 3(c)–3(e) and 4(e)]. Figure 4(g) presents the emission spectra for all seven combinations; Fig. 4(h) shows the calculated chromaticity for each of the lasing spectra in a CIE (Commission Internationale de L'Eclairage)1931 color diagram (red, green, blue, yellow, cyan, magenta, and white, respectively). In addition, according to Grassmann's law, all colors inside the triangle pattern formed by the three elementary colors can be realized through appropriate mixing of the three colors. The chromaticity of the carefully balanced white lasing is very close to that of the white point of the CIE standard white illuminant D65 [30] [Fig. 4(h)].

Further evidence for multicolor lasing behavior can be seen for each of the three RGB colors [Fig. 4(g)] in the light-in−light-out curves [inset Figs. 5(a)–5(c)], together with the theoretical fittings based on lasing equations [24]. One can see typical J-like curves covering the three colors of operation. From the experimental data, we demonstrate a lasing wavelength span of 1 nm when only one peak in the spontaneous emission is observed. As pumping intensity increases, a broadband of spontaneous emission is observed. From the spectral evolution as a function of the pumping energy [Fig. 5(d)], only a broadband of spontaneous emission is observed at the lowest pumping energy (<23 mW). In the energy range from 23 to 28 mW, narrow peaks at 636 (red), 423 (blue), and 530 nm (green) appear sequentially. The intensity of each color increases with pumping energy and is attributable to the well-known lasing behavior of the corresponding dye.

To illustrate the potential of our hybrid microcavity for general illumination, we study the dynamic tuning of color blending over the full color range and also the white-light lasing in particular. The three beams are focused into long,

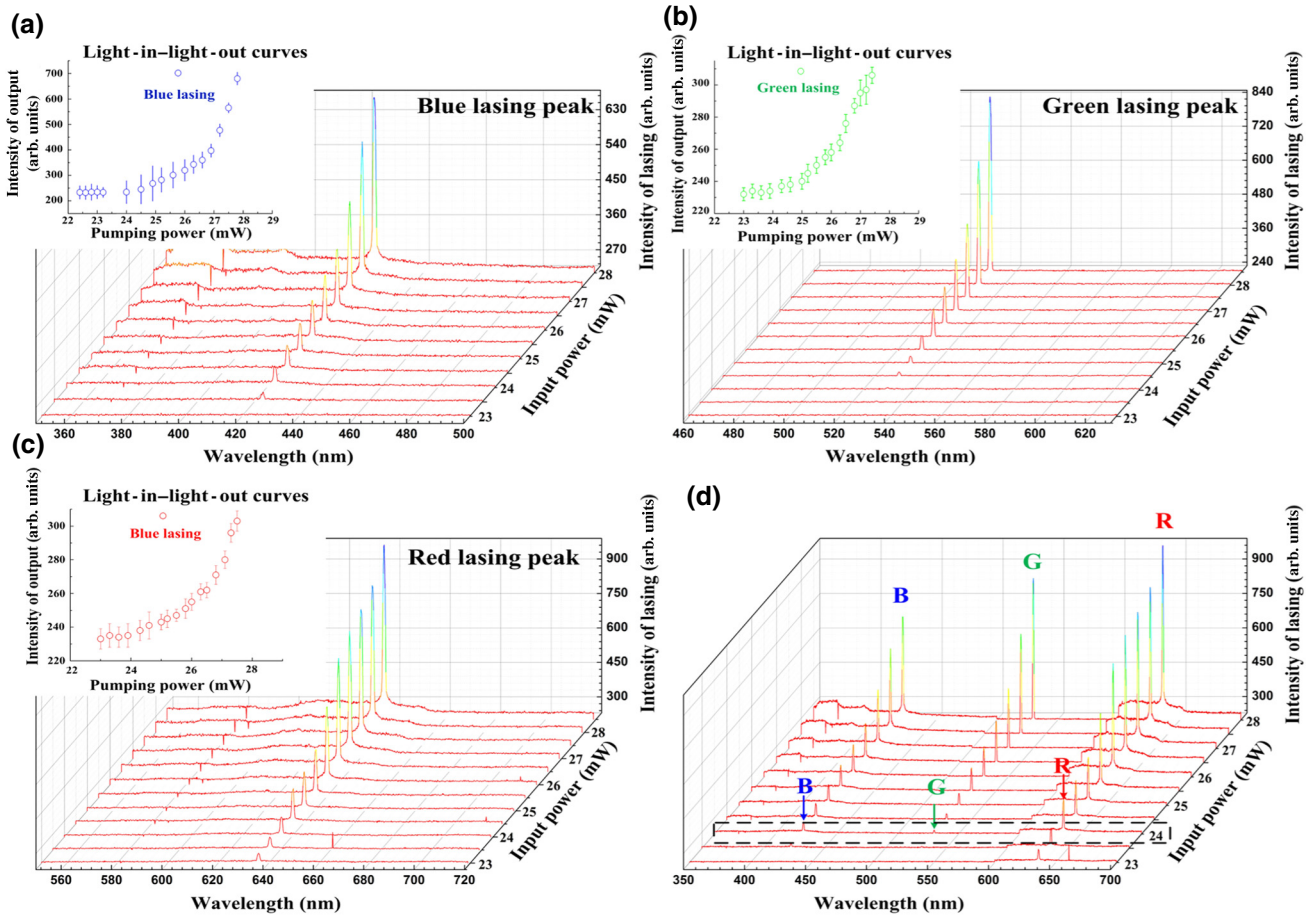

FIG. 5. Fitted light-in–light-out curves with multimode lasing: (a)–(c) for the 423, 530, and 636 nm lasing peaks. Inset: plots of the curves at threshold. (d) RGB lasing peaks are excited with pumping on the triple slab-capillary microcavity chip.

narrow, parallel stripes to pump one of the three capillaries accordingly. The power of each pumping beam is adjustable, allowing for a precise independent tuning of the lasing intensity for each color. As a result, color-blended lasing in the far field is controlled over the full-color range and the desired white light is achieved. The results are summarized in Fig. 6. A photo luminescence image and the structure of the hybrid microcavity are given in Figs. 4(c) and 4(d). By pumping above the lasing threshold and injecting two different dye solutions into two capillaries of

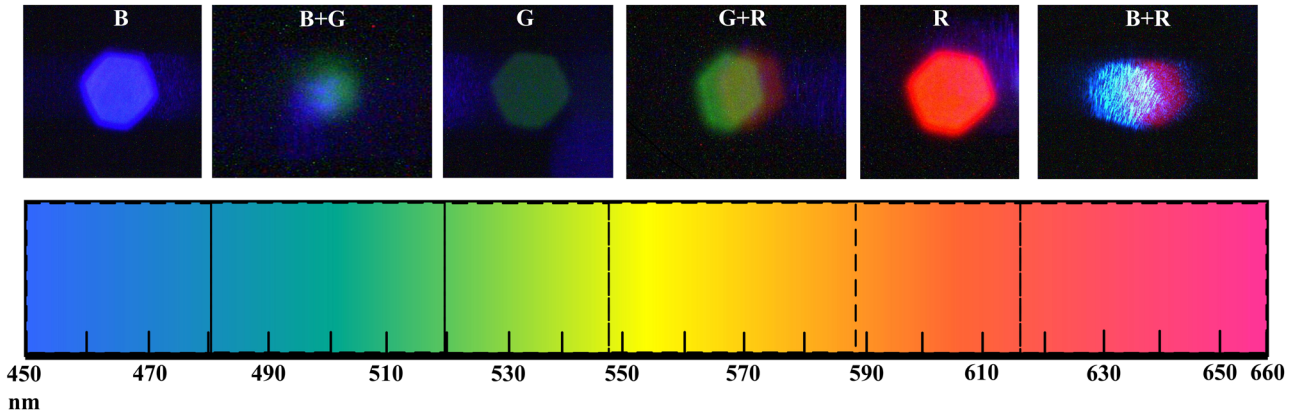

FIG. 6. Full-color tunable lasing. The triple metal-cladded slab-capillary microcavity chip in which the three capillaries are placed side by side. The S-420, C-540, and R-610 dye solutions are injected into their respective capillaries. Adjusting the inclination of the capillaries, two colors of the RGB lasing points are made to converge to a point to produce different color lasing points.

the chip, we demonstrate independent lasing of each primary color, the simultaneous two-color lasing of any two of three primary colors, and finally, simultaneous lasing of all three—that is, RGB lasing.

V. CONCLUSION

We demonstrate simultaneous RGB lasing from individual multichannel hybrid microcavities at room temperature. White light and tunable lasing over the full range of visible colors is achieved with controlled injection of different dye solutions into metal-cladded capillaries of a microcavity. The essence in our demonstration is the development of a unique growth strategy that exploits the interplay of the vertical launching system, slab waveguide, and mode-cross-coupling to a capillary. Through a detailed characterization and understanding of this emission mechanism, we design an optimized multichannel hybrid microcavity that allows incident light to be coupled into a slab waveguide layer and a hollow-core capillary with the desired thickness of metal cladding, pumping wavelength, and capillary length. The metal-cladded film significantly increases the absorption of off-resonance photons and couples resonance photons to a high-density power field in the capillary interior. As a result, lasing with a line width of approximately 1 nm in a hybrid microcavity structure, the largest ever reported, is observed. Our results demonstrate that the apparently contradictory concepts "white light" and "lasing" can both be realized in a single structure. Our work dramatically simplifies the process of creating monolithic laser structures with dynamic color-controllable emissions, and is an important step toward the realization of an electrically driven microlaser for white light and full-color beams from a single monolithic structure.

ACKNOWLEDGMENTS

This work was supported by the National Key R&D Program of China (Grant No. 2018YFA0306301, 2017YFA0303701); National Natural Science Foundation of China (NSFC) (Grant No. 11734011); The Foundation for Development of Science and Technology of Shanghai (Grant No. 17JC1400400).

[1] Fan Qian, Yat Li, Silvija Gradečak, Hong-Gyu Park, Yajie Dong, Yong Ding, Zhong Lin Wang, and Charles M. Lieber, Multi-quantum-well nanowire hetero structures for wavelength controlled lasers, Nature **7**, 701 (2008).

[2] Cuong Dang, Joonhee Lee, Craig Breen, Jonathan S. Steckel, Seth Coe-Sullivan, and Arto Nurmikko, Red, green and blue lasing enabled by single-exaction gain in colloidal quantum dot films, Nat. Nanotechnol. **7**, 335 (2012).

[3] Kenichi Yamashita, Nobutaka Takeuchi, Kunishige Oe, and Hisao Yanagi, Simultaneous RGB lasing from a single-chip polymer device, Opt. Lett. **35**, 2451 (2010).

[4] Sindy K. Y. Tang, Zhenyu Li, Adam R. Abate, Jeremy J. Agresti, David A. Weitz, Demetri Psaltis, and George M. Whitesides, A multi-color fast-switching microfluidic droplet dye laser, Lab Chip **9**, 2767 (2009).

[5] Ye Ding, Qing Yang, Xin Guo, Shanshan Wang, Fuxing Gu, Jian Fu, Qing Wan, Jipeng Cheng, and Limin Tong, Nanowires/micorfibre hybrid structure multicolor laser, Opt. Express **17**, 21813 (2009).

[6] Shujing Chen, Xiaoye Zhao, Yanrong Wang, Jinwei Shi, and Dahe Liu, White light emission with red green-blue lasing action in a disordered system of nanoparticles, Appl. Phys. Lett. **101**, 123508 (2012).

[7] Nader A. Naderi, Frédéric Grillot, Kai Yang, Jeremy B. Wright, Aaron Gin, and Luke F. Lester, Two-color multi-section quantum dot distributed feedback laser, Opt. Express **18**, 27026 (2010).

[8] A. P. Alivisatos, Semiconductor clusters, nanocrystals, and quantum dots, Science **271**, 933 (1996).

[9] Jonathan J. Wierer, Jr., Jeffrey Y. Tsao, and Dmitry S. Sizov, Comparison between blue laser and light-emitting diodes for future solid-state lighting, Laser Photon. Rev. **7**, 963 (2013).

[10] Akira Kotani, Małgorzata A. Witek, John K. Osiri, Hong Wang, Rondedrick Sinville, Hanna Pincas, Francis Barany, and Steven A. Sope, EndoV/DNA ligase mutation scanning assay using microchip capillary electrophoresis and dual-color laser-induced fluorescence detection, Anal. Methods **4**, 58 (2012).

[11] M. L. Pascu, N. Moise, and A. Staicu, Tunable dye laser applications in environment pollution monitoring, J. Mol. Struct. **598**, 57 (2001).

[12] Yu Huang, Xiangfeng Duan, and Charles M. Lieber, Nanowires for integrated multicolor nanophotonics, Small **1**, 142 (2005).

[13] Tevye Kuykendall, Philipp Ulrich, Shaul Aloni, and Peidong Yang, Complete composition tunability of InGaN nanowires using a combinatorial approach, Nat. Mater. **6**, 951 (2007).

[14] Zongyin Yang, Jinyou Xu, Pan Wang, Xiujuan Zhuang, Anlian Pan, and Limin Tong, On-nanowire spatial band gap design for white light emission, Nano Lett. **11**, 5085 (2011).

[15] Tae-Ho Kim, Kyung-Sang Cho, Eun Kyung Lee, Sang Jin Lee, Jungseok Chae, Jung Woo Kim, Do Hwan Kim, Jang-Yeon Kwon, Gehan Amaratunga, Sang Yoon Lee, Byoung Lyong Choi, Young Kuk, Jong Min Kim, and Kinam Kim, Full-colour quantum dot displays fabricated by transfer printing, Nat. Photon. **5**, 176 (2011).

[16] F. Fan, Z. Liu, L. Yin, P. L. Nichols, H. Ning, S. Turkdogan, and C. Z. Ning, Simultaneous two-color lasing in a single CdSSe heterostructure nanosheet, Semicond. Sci. Technol. **28**, 065005 (2013).

[17] Zhicheng Liu, Leijun Yin, Hao Ning, Zongyin Yang, Limin Tong, and Cun-Zheng Ning, Dynamical color-controllable lasing with extremely wide tuning range from red to green in a single alloy nanowire using nanoscale manipulation, Nano Lett. **13**, 4945 (2013).

[18] Yu Lee Kim, Jae Hun Jung, Hyun Sik Yoon, Man Suk Song, Se Hwan Bae, Yong Kim, Zhi Gang Chen, Jin

Zou, Hannah J Joyce, Qiang Gao, Hark Hoe Tan, and Chennupati Jagadish, CdS/CdSe lateral heterostructure nanobelts by a two-step physical vapor transport method, Nanotechnology **21**, 145602 (2010).

[19] Xiaosheng Fang, Tianyou Zhai, Ujjal K. Gautam, Liang Li, Limin Wu, Yoshio Bando, and Dmitri Golberg, ZnS nanostructures: From synthesis to applications, Prog. Mater. Sci. **56**, 175 (2011).

[20] Dong Hee Son, Steven M. Hughes, Yadong Yin, and A. Paul Alivisatos, Cation exchange reactions in ionic nanocrystals, Science **306**, 1009 (2004).

[21] Hailang Dai, Bei Jiang, Cheng Yin, Zhuangqi Cao, and Xianfeng Chen, Ultralow-threshold continuous-wave lasing assisted by a metallic optofluidic cavity exploiting continuous pump, Opt. Lett. **43**, 847 (2018).

[22] Wen Yuan, Cheng Yin, Pingping Xiao, Xianping Wang, Jingjing Sun, Sang Minghuang, Xianfeng Chen, and Zhuangqi Cao, Microsecond-scale switching time of magnetic fluids due to the optical trapping effect in waveguide structure, Microfluid Nanofluid **11**, 781 (2011).

[23] Wen Yuan, Cheng Yin, Honggen Li, Pingping Xiao, and Zhuangqi Cao, Wideband slow light assisted by ultrahigh-order modes, J.O.S.A. B **28**, 968 (2011).

[24] Hailang Dai, Cheng Yin, Xiaona Ye, Bei Jiang, Maowu Ran, Zhuangqi Cao, and Xianfeng Chen, A possible pathogenetic factor of sickle-cell disease based on fluorescent analysis via an optofluidic resonator, Sci. Rep. **7**, 3174 (2017).

[25] Fan Chen, Zhuangqi Cao, Qishun Shen, and Yaojun Feng, Optical approach to angular displacement measurement based on attenuated total reflection, Appl. Opt. **13**, 10061 (2005).

[26] Yi Wang, Zhuangqi Cao, Tianyi Yu, Honggen Li, and Qishun Shen, Enhancement of the superprism effect based on the strong dispersion effect of ultrahigh-order modes, Opt. Lett. **33**, 1276 (2008).

[27] Honggen Li, Zhuangqi Cao, Haifeng Lu, and Qishen Shen, Free-space coupling of a light beam into a symmetrical metal-cladding optical waveguide, Appl. Phys. Lett. **83**, 2757 (2003).

[28] Bei Jiang, Hailang Dai, and Xianfeng Chen, Enhancement of stimulated emission by a metallic optofluidic resonator, Photon. Res. **6**, 597 (2018).

[29] Yuanlin Zheng, Zhuangqi Cao, and Xianfeng Chen, Conical reflection of light during free-space coupling into a symmetrical metal-cladding waveguide, J.O.S.A. A **30**, 1901 (2013).

[30] International Commission on Illumination, *CIE 15 Colorimetry Technical Report*, 3rd edn, US Government Document (International Commission on Illumination, 2004).